5. Kurata J. A potential role of functional magnetic resonance imaging in the diagnosis of pain. Jpn J Anesthesiol. 2009;58: 1350–9. (in Japanese with English abstract).
6. Seifert F, Jungfer I, Schmelz M, Maihofner C. Representation of UV-B-induced thermal and mechanical hyperalgesia in the human brain: a functional MRI study. Hum Brain Mapp. 2008; 29:1327–42.
7. Borsook D, Moulton EA, Tully S, Schmahmann JD, Becerra L. Human cerebellar responses to brush and heat stimuli in healthy and neuropathic pain subjects. Cerebellum. 2007;22:1–21.
8. Niddam DM, Yeh TC, Wu YT, Lee PL, Ho LT, Arendt-Nielsen L, Chen AC, Hsieh JC. Event-related functional MRI study on central representation of acute muscle pain induced by electrical stimulation. Neuroimage. 2002;17:1437–50.
9. Henderson LA, Bandler R, Gandevia SC, Macefield VG. Distinct forebrain activity patterns during deep versus superficial pain. Pain. 2006;120:286–96.
10. Svensson P, Minoshima S, Beydoun A, Morrow TJ, Casey KL. Cerebral processing of acute skin and muscle pain in humans. J Neurophysiol. 1997;78:450–60.
11. Kobayashi Y, Kurata J, Sekiguchi M, Kokubun M, Akaishizawa T, Chiba Y, Konno S, Kikuchi S. Augmented cerebral activation by lumbar mechanical stimulus in chronic low back pain patients: an FMRI study. Spine. 2009;34:2431–6.
12. Gracely RH, Petzke F, Wolf JM, Clauw DJ. Functional magnetic resonance imaging evidence of augmented pain processing in fibromyalgia. Arthritis Rheum. 2002;46:1333–43.
13. Talairach J, Tournoux P. Co-planar stereotactic atlas of the human brain: 3-dimensional proportional system—an approach to cerebral imaging. New York: Thieme; 2002.
14. Nie H, Arendt Nielsen L, Andersen H, Graven Nielsen T. Temporal summation of pain evoked by mechanical stimulation in deep and superficial tissue. J Pain. 2005;6:348–55.
15. Mach DB, Rogers SD, Sabino MC, Luger NM, Schwei MJ, Pomonis JD, Keyser CP, Clohisy DR, Adams DJ, O'Leary P, Mantyh PW. Origins of skeletal pain: sensory and sympathetic innervation of the mouse femur. Neuroscience. 2002;113:155–66.
16. Korotkov A, Radovanovic S, Ljubisavljevic M, Lyskov E, Kataeva G, Roudas M, Pakhomov S, Thunberg J, Medvedev S, Johansson H. Comparison of brain activation after sustained non-fatiguing and fatiguing muscle contraction: a positron emission tomography study. Exp Brain Res. 2005;163:65–74.
17. Coghill RC, Sang CN, Maisog JM, Iadarola MJ. Pain intensity processing within the human brain: a bilateral, distributed mechanism. J Neurophysiol. 1999;82:1934–43.
18. Ringler R, Greiner M, Kohlloeffel L, Handwerker HO, Forster C. BOLD effects in different areas of the cerebral cortex during painful mechanical stimulation. Pain. 2003;105:445–53.
19. Bingel U, Glascher J, Weiller C, Buchel C. Somatotopic representation of nociceptive information in the putamen: an event-related fMRI study. Cereb Cortex. 2004;14:1340–5.
20. Doyon J, Bellec P, Amsel R, Penhune V, Monchi O, Carrier J, Lehericy S, Benali H. Contributions of the basal ganglia and functionally related brain structures to motor learning. Behav Brain Res. 2009;199:61–75.
21. Marchand WR. Cortico-basal ganglia circuitry: a review of key research and implications for functional connectivity studies of mood and anxiety disorders. Brain Struct Funct. 2010;215:73–96.
22. Grahn JA, Parkinson JA, Owen AM. The role of the basal ganglia in learning and memory: neuropsychological studies. Behav Brain Res. 2009;199:53–60.
23. Chudler EH, Dong WK. The role of the basal ganglia in nociception and pain. Pain. 1995;60:3–38.

Neuroscience Research 70 (2011) 78–84

Contents lists available at ScienceDirect

Neuroscience Research

journal homepage: www.elsevier.com/locate/neures

Brain imaging of mechanically induced muscle versus cutaneous pain

Hironobu Uematsu[a,*], Masahiko Shibata[b], Satoru Miyauchi[c,d], Takashi Mashimo[a]

[a] Department of Anesthesiology and Intensive Care Medicine, Osaka University Graduate School of Medicine, 2-2 Yamadaoka, Suita, Osaka 565-0871, Japan
[b] Department of Pain Medicine, Osaka University Graduate School of Medicine, Osaka, Japan
[c] CREST Brain Function Imaging Team, Kobe Advanced ICT Research Center, National Institute of Information and Communications Technology (NICT), Hyogo, Japan
[d] CREST, Japan Science and Technology Agency (JST), Saitama, Japan

ARTICLE INFO

Article history:
Received 12 November 2010
Received in revised form 14 January 2011
Accepted 24 January 2011
Available online 1 February 2011

Keywords:
Functional MRI
Cutaneous pain
Muscle pain
Mechanical stimulation
Local anesthesia
Secondary somatosensory cortex
Insular cortex
Cingulate cortex

ABSTRACT

This study aimed to investigate the differences in the brain responses between muscle versus skin pain, both of which were caused by tonic mechanical stimuli. Using local anesthesia (LA), we induced muscle pain without any accompanying cutaneous sensation. Subjects underwent functional magnetic resonance imaging while tonic pressure was applied to the right calf under the following four conditions: (1) non-painful pressure without LA (causing mechanoreceptive skin and muscle stimulation); (2) painful pressure without LA (causing nociceptive skin stimulation and mechanoreceptive skin and muscle stimulation); (3) non-painful pressure with LA (causing mechanoreceptive muscle stimulation); (4) painful pressure with LA (causing nociceptive and mechanoreceptive muscle stimulation). Although there was no brain region specifically activated by nociceptive muscle stimuli, activation in the following regions was observed specifically during nociceptive muscle stimuli: anterior midcingulate cortex, anterior and posterior insular cortex, lentiform nucleus, thalamus, pre-supplementary motor area, dorsolateral prefrontal cortex, and inferior parietal lobule. This indicates that there is no region specific for muscle pain but activation pattern or network specific for muscle pain. Furthermore, secondary somatosensory cortex (S2) was found to be responsive to cutaneous pain, not muscle pain, because S2 was specifically activated by nociceptive cutaneous stimuli.

1. Introduction

Pathological muscle pain is much more frequently encountered in clinical practice than is superficial cutaneous pain, and its treatment poses a bigger challenge. It has a significant impact on individuals and societies, as well as healthcare services and economies (Suka and Yoshida, 2005). However, the central processing pathways for muscle pain have been less explored than those of cutaneous pain (Sung et al., 2007; Borsook et al., 2008; Seifert et al., 2008). The typical characteristics of pathological muscle pain are mechanical nociception-related pain; i.e., muscle tenderness, pressure and movement-related pain (Staud et al., 2003). As such, studies of mechanically induced muscle pain are required to link the experimental findings from neuroimaging studies with clinical interpretations. Nevertheless, to date there are no functional imaging studies of muscle pain using mechanical stimulation. A classical functional imaging study of muscle pain using phasic electrical stimulation suggested a common representation for both thermally induced cutaneous pain and electrically induced muscle pain (Svensson et al., 1997). More recently, a few studies using tonic muscle stimuli, such as electric stimulation and injection of hypertonic saline or acidic saline, showed distinct temporal activity patterns of the tonic state comparing experimental skin and muscle pain (Schreckenberger et al., 2005; Henderson et al., 2006; Owen et al., 2010). Stimuli such as electric stimulation and injection of hypertonic saline, however, are not physiological energy forms (thermal, mechanical or chemical), and injection of acidic saline includes two forms of stimulus energy (mechanical and chemical). In this regard, studies using such non-physiological stimuli can clarify roles of temporal activity patterns in experimental skin versus muscle pain processing, but only studies using mechanical stimuli can properly link the experimental findings with clinical interpretations.

One of the reasons so few investigators have studied mechanically induced muscle pain is that under normal circumstances, mechanical stimulation to the muscle is always accompanied by cutaneous stimulation (Nie et al., 2005). To resolve this methodological issue, a few recent psychophysical studies used local anesthesia (LA) to stimulate the muscle without any sensation to

Abbreviations: LA, local anesthesia; fMRI, functional magnetic resonance imaging; IPL, inferior parietal lobule; S2, secondary somatosensory cortex; preSMA, pre-supplementary motor area; aMCC, anterior mid-cingulate cortex; aIC, anterior insular cortex; pIC, posterior insular cortex; DLPFC, dorsolateral prefrontal cortex; LN, lentiform nucleus.

* Corresponding author. Tel.: +81 6 6879 3745; fax: +81 6 6879 3495.
E-mail address: Uhironobu@anes.med.osaka-u.ac.jp (H. Uematsu).

0168-0102/$ – see front matter © 2011 Elsevier Ireland Ltd and the Japan Neuroscience Society. All rights reserved.
doi:10.1016/j.neures.2011.01.015

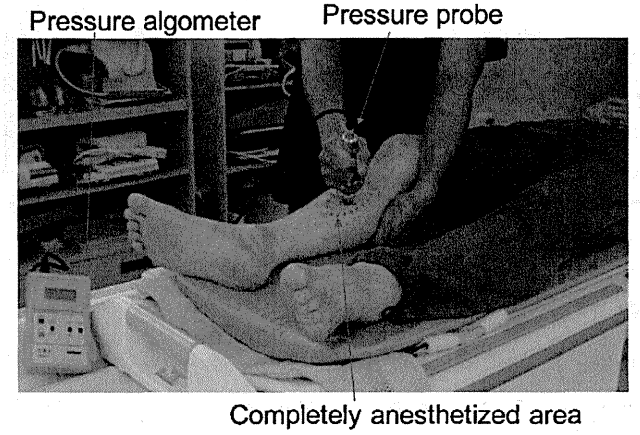

Fig. 1. A pressure probe (diameter, 10 mm) was pressed down perpendicularly to the skin surface over the right calf (gastrocnemius muscle) from the medial side (the periosteum was not stimulated). The experimenter was trained to operate the probe before the experiments so that the pressure was stably maintained and the rate of pressure increase was kept constant. We injected 2 ml of lidocaine (AstraZeneca, Xylocaine® Injection syringe 1%) subcutaneously over the right calf (gastrocnemius muscle) in order to anesthetize the skin completely. We marked the area that was completely anesthetized (at least 3 cm × 3 cm), and all mechanical stimuli were applied in this region.

the skin (Graven-Nielsen et al., 2004; Takahashi et al., 2005). In the present study, we investigated the differences in the brain responses between muscle versus skin pain, both of which were caused by tonic mechanical stimuli, using LA in combination with functional magnetic resonance imaging (fMRI).

2. Materials and methods

2.1. Subjects

Seventeen healthy volunteers (10 males, 7 females, age range 23–33) participated in this study. None of the subjects had any neurological illness or detectable MRI abnormalities. They agreed to receive painful pressure during fMRI scanning. The study was approved by the Osaka University Hospital Institutional Review Board, and written informed consent was obtained from each subject before the experiment. All experiments were conducted in accordance with the Declaration of Helsinki.

2.2. Experimental protocol

A pressure hemispherical probe (diameter, 10 mm) was pressed down perpendicularly to the skin surface over the right calf (gastrocnemius muscle) from the medial side (the periosteum was not stimulated) (Fig. 1). This probe was attached to an electronic pressure algometer (Pressure Algometer NPA-1, Shinko, Japan), which measured the pressure in Newtons (N). The apparatus was held and moved manually. The experimenter was trained to operate the probe before the experiments so that the pressure was stably maintained and the rate of pressure increase was kept constant.

As shown in Table 1, the four experimental conditions were as follows: (A) 10 N pressure *without* LA, causing mechanoreceptive skin and muscle stimulation, but no pain sensation; (B) 20 N pressure *without* LA, causing mechanoreceptive skin and muscle stimulation and pain sensation in skin only; (C) 10 N pressure *with* LA, causing mechanoreceptive muscle stimulation and no pain sensation; and (D) 30 N pressure *with* LA, causing mechanoreceptive and nociceptive muscle stimulation, which resulted in muscle pain without any skin sensation. The pressure intensities in each condition were defined on the basis of the results of the preliminary experiment in which six participants evaluated non-painful and painful sensation in the skin and in the muscle induced by various pressure stimuli (data not shown). The reason why we did not apply the same pressure in Conditions B and D was because some participants were not able to tolerate 30 N pressure without LA in a preliminary experiment. In addition, although the order of Conditions A/B or C/D was pseudo-randomly balanced among all subjects, we performed the conditions without LA (Conditions A and B) before the conditions with LA (Conditions C and D) to avoid the possibility of a lingering effect from the anesthesia.

Table 1
Four experimental conditions.

Condition	Local anesthesia	Pressure (N)	Pain sensation	Region of painful stimulation	Region of mechanosensory stimulation
A	–	10	–	–	Skin + muscle
B	–	20	+	Skin	Skin + muscle
C	+	10	–	–	Muscle
D	+	30	+	Muscle	Muscle

The experimental paradigm consisted of interleaved rest (40 s) and activation (20 s) phases, leading to a total scanning time of 6 min in each session (7 rest plus 6 activation phases). Time intervals between sessions were at least 1 min, and two sessions were delivered within each condition. There was a 20-s rest period before the first activation, as well as after the last activation, of each session. A total of 8 sessions (48 min) were acquired per subject. The exact location of each probe application was slightly changed throughout the 8 sessions so as not to over-stimulate the same point on the calf.

2.3. Local anesthesia

We injected 2 ml of lidocaine (AstraZeneca, Xylocaine® Injection syringe 1%) subcutaneously over the right calf (gastrocnemius muscle) in order to anesthetize the skin completely, which enabled us to limit stimulation to muscle in Conditions C and D. To assess skin sensation, we applied pin-prick and cold stimuli to the anesthetized skin surface using a stainless steel needle and an 81.4% ethyl alcohol solution. These assessments were performed at least 5 min before and after scanning. We marked the area that was completely anesthetized (at least 3 cm × 3 cm), and all mechanical stimuli were applied in this region.

2.4. Pain intensity rating

The subjective pain intensity was assessed after every session in Conditions B and D. Subjects were asked to rate the mean intensity of pain using a numerical rating scale (NRS) that was defined as follows: 0 = no pain, 10 = worst pain imaginable.

2.5. Functional MRI procedures

A 1.5-T MRI scanner (Signa EXCITE XI 11.0, GE Healthcare, Milwaukee, WI) was used to detect the blood oxygenation level-dependent (BOLD) contrast. fMRI scans were acquired using echo-planar imaging sequences (gradient echo; repetition time [TR], 2500 ms; echo time [TE], 60 ms; flip angle [FA], 90; field of view [FOV], 300 mm; in-plane resolution, 4.69 mm × 4.69 mm; 30 slices of 5 mm thickness, no gap). An interleaved scanning sequence was used. All subjects were positioned in the scanner with a foam rubber pad to minimize head movement and instructed simply to lay with their eyes closed without moving or talking. High-resolution T1-weighted anatomical images with the same orientation as the EPI slices were collected from each subject.

2.6. Data analysis

Statistical parametric mapping (SPM2, Wellcome Department of Cognitive Neurology, London, UK) implemented in Matlab 7 (Mathworks Inc., Sherborn, MA) was used for preprocessing (realignment, normalization, and smoothing [10-mm isotropic Gaussian kernel]; high-pass filter cutoff to 128 s) and statistical analysis of the fMRI data. We used global mean scaling to remove confounding global effects on local signals. To make statistical inferences at the population level, individual data sets were then summarized and incorporated into a random-effects model ($p < 0.005$, uncorrected for multiple comparisons; with cluster size $k > 20$ voxels). To identify statistically significant differences between non-painful and painful conditions, a comparison was conducted with a paired t-test of contrast images ($p < 0.005$, uncorrected for multiple comparisons; with cluster size $k > 20$ voxels): comparison B–A indicates areas showing significant differences in activation in Condition B versus A; comparison D–C indicates areas showing significant differences in activation in Condition D versus C. Since accumulating evidence exists for an *a priori* 'pain matrix' for experimental stimuli (Peyron et al., 2000), we hypothesized that the anatomical structures involved in previous experimental pain were also involved in mechanically induced skin and muscle pain. For the areas with an *a priori* pain-related hypothesis (Svensson et al., 1997; Niddam et al., 2002; Schreckenberger et al., 2005; Henderson et al., 2006; Owen et al., 2010), we applied lenient height and extent thresholds ($p < 0.005$ uncorrected and $k > 20$ (Helmchen et al., 2003; Raij et al., 2005; Moriguchi et al., 2007) within the regions activated in a random-effect analysis and paired t-tests reduced the risk of false negatives. If the regions with the activation and significant differences were included in an *a priori* 'pain matrix' confirmed by previous studies (Svensson et al., 1997; Peyron et al., 2000; Niddam et al., 2002; Schreckenberger et al., 2005; Henderson et al., 2006; Owen et al., 2010), we considered them significant for regionally specific activation and differences associated with mechanically induced skin and muscle pain.

3. Results

3.1. Intensity ratings

The mean pain intensity ratings were as follows: Condition B = 5.8 ± 1.3 (mean ± SEM); Condition D = 4.7 ± 1.7. There were no statistically significant differences in the mean pain intensity ratings between painful Conditions B and D (Wilcoxon's test; $p > 0.05$).

3.2. Brain regions activated by painful stimulation

The common regions activated in all conditions were bilateral pre-supplementary motor area (preSMA), bilateral dorsolateral prefrontal cortex (DLPFC), and bilateral inferior parietal lobule (IPL). Bilateral thalami were activated by painful pressure (Conditions B and D). Bilateral anterior insular (aIC), contralateral posterior insular cortex (pIC), bilateral anterior midcingulate cortex (aMCC) and bilateral lentiform nucleus (LN) were activated in all conditions except Condition C. Bilateral secondary somatosensory cortex (S2) activation was observed in Condition B only (Fig. 2, Table 2).

The S2 (bilateral), pIC (contralateral) and the thalamus (bilateral) were significantly more activated in Condition B than in Condition A (Fig. 2 B–A, Table 3), whereas the aMCC (bilateral), aIC (contralateral) and pIC (contralateral), LN (contralateral), thalamus (bilateral), DLPFC (bilateral), IPL (bilateral) and preSMA (bilateral) were significantly more activated in Condition D than in Condition C (Fig. 2D–C, Table 3).

4. Discussion

In the present study, we used LA in order to anesthetize the skin, which enabled us to mechanically stimulate the muscle without any sensation to the skin, and to directly examined brain responses to mechanically induced muscle pain with fMRI.

4.1. The activation pattern specific to muscle pain

If there are brain regions specifically associated with muscle pain, then they should be specifically activated in Condition D, in which nociceptive stimuli were selectively delivered to the muscle. Although aMCC, aIC, pIC, LN, thalamus, DLPFC, IPL and preSMA were activated in Condition D, these regions were also activated in some other conditions, suggesting that there is no region specific to muscle pain. However, the activation patterns were considerably different across conditions, indicating that while there is no region that specifically processes muscle pain, there may be an activation pattern or network specific to muscle pain. That is, concurrent activation of these multiple regions (aMCC, aIC, pIC, LN, thalamus, DLPFC, IPL and preSMA) could be associated with muscle pain, specifically. In accordance with this idea, Tracey (2005) also suggests that the emergence of pain would not result from the activation of one or more specific brain areas but would emerge from the 'flow and integration of information' among the structures of the Pain Matrix that constitutes, as an ensemble, the neural substrate for pain perception (Tracey, 2005).

Regions activated in Condition D can be divided into two subsets: regions that were not also activated in Condition C (aMCC, aIC and pIC) and regions that were activated in both Conditions C and D (DLPFC, IPL and preSMA). In Condition D, nociceptive stimuli to the muscle were delivered in addition to mechanoreceptive stimuli to the muscle, as were applied in Condition C. Since aMCC, aIC and pIC were activated in Condition D and not activated in Condition C, these regions could be directly associated with muscle pain processing. Previous studies that employed different types of experimental stimuli to the muscle itself (intramuscular injections of hypertonic saline or acidic saline) also suggested that these regions are responsive to muscle pain (Schreckenberger et al., 2005; Henderson et al., 2006; Owen et al., 2010). Further, it was recently reported that the temporal activity patterns in aMCC and aIC are related to muscle pain with the affective response, while that in pIC is responsible for pain intensity rating (Owen et al., 2010). These imply that aMCC, aIC and pIC would be main structures of the activation pattern specific for muscle pain where the affective or sensory-discriminative components of pain perception are implicated. On the other hand, DLPFC, IPL and preSMA were activated in both Conditions C and D. This indicates that these regions are not directly associated with muscle pain processing. In previous studies, these regions did not seem to be the regions directly associated with pain processing, but rather the structures associated with non-specific cognition and multimodal processing (Qiu et al., 2006; Oshiro et al., 2007). Taking all of these results into consideration, muscle pain would result from the concurrent activation of regions directly associated with muscle pain processing (aMCC, aIC and pIC) and regions associated with non-specific cognition or multimodal processing (DLPFC, IPL and preSMA).

4.2. The role of S2 in pain perception

Another notable finding in this study is that S2 was activated in Condition B only. Since it was not possible to mechanically stimulate the skin itself without any sensation to the muscle, S2 activation might have responded to nociceptive skin stimuli and/or mechanoreceptive muscle stimuli. However, S2 was not activated in Conditions C and D, in which LA blocked skin sensation. This

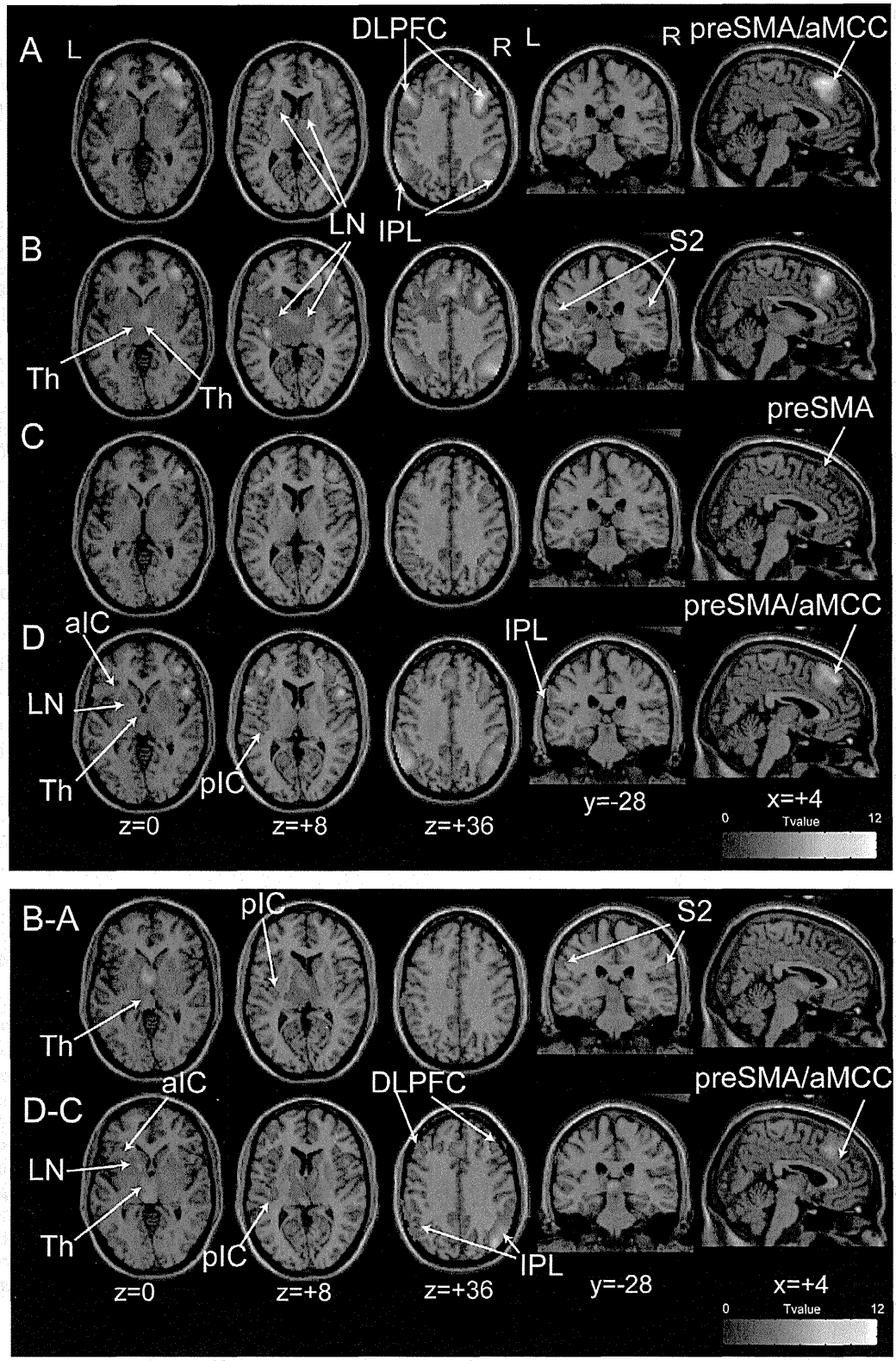

Fig. 2. Panels A–D show the brain regions activated in each condition: A, mechanoreceptive stimuli to skin and muscle (without local anesthesia [LA]); B, nociceptive stimuli to the skin and mechanoreceptive stimuli to the skin and muscle (without LA); C, mechanoreceptive stimuli to the muscle (with LA); D, mechanoreceptive stimuli to the muscle and nociceptive stimuli to the muscle (with LA). Panels B–A show the regions significantly more activated in Condition B than in Condition A. Panels D–C show the regions significantly more activated in Condition D than in Condition C. Activated regions were overlaid on the T1-weighted MNI single-subject template. The color of each activated voxel corresponds to its *T*-value, as per the color bar scales ($n = 17$, height and extent thresholds; $p < 0.005$ uncorrected for multiple comparison and cluster size $k > 20$ voxels). IPL, inferior parietal lobule; S2, secondary somatosensory cortex; preSMA, pre-supplementary motor area; aMCC, anterior mid-cingulate cortex; aIC, anterior insular cortex; pIC, posterior insular cortex; DLPFC, dorsolateral prefrontal cortex; Th, thalamus; LN, lentiform nucleus; L, left side (contralateral to the stimulation); R, right side (ipsilateral to the stimulation).

Table 2
Coordinates (MNI) of regions activated in Conditions A–D.

Region	Condition A				
	Voxels	*x*	*y*	*z*	*T*-value
Right inferior parietal lobule	4115	54	−48	54	10.07
Left inferior parietal lobule	2592	−54	−46	52	9.55
Right pre-supplementary motor area	3275	4	30	54	11.74
Right anterior mid-cingulate cortex		6	26	40	7.13
Left pre-supplementary motor area		−8	28	48	8.40
Left anterior mid-cingulate cortex		−10	22	46	5.27
Right anterior insular cortex	597	38	22	−4	5.22
Left anterior insular cortex	286	−44	14	4	4.69
Left posterior insular cortex	295	−36	−24	8	5.30
Right dorsolateral prefrontal cortex	5382	42	38	24	6.03
Left dorsolateral prefrontal cortex	4065	−50	32	34	6.31
Right lentiform nucleus	329	−12	8	−4	3.99
Left lentiform nucleus	328	−16	12	0	4.04
Region	Condition B				
	Voxels	*x*	*y*	*z*	*T*-value
Right inferior parietal lobule	2016	52	62	38	7.02
Right secondary somatosensory cortex		54	−30	24	5.78
Left inferior parietal lobule	2395	−60	−58	34	6.03
Left secondary somatosensory cortex		−56	−30	22	5.81
Right pre-supplementary motor area	3641	6	32	52	10.07
Right anterior mid-cingulate cortex		6	26	36	6.05
Left pre-supplementary motor area		−8	32	50	7.73
Left anterior mid-cingulate cortex		−4	26	36	5.02
Right anterior insular cortex	608	44	14	4	3.45
Left anterior insular cortex	838	−38	8	8	3.14
Left posterior insular cortex		−34	−20	10	7.31
Right dorsolateral prefrontal cortex	4592	36	16	34	6.73
Left dorsolateral prefrontal cortex	3656	−38	4	38	4.47
Right lentiform nucleus	176	8	2	−2	4.10
Left lentiform nucleus	352	−12	−2	2	3.94
Right thalamus	351	2	−6	6	4.84
Left thalamus	364	−2	−6	6	4.66
Region	Condition C				
	Voxels	*x*	*y*	*z*	*T*-value
Right inferior parietal lobule	852	56	−44	52	5.05
Left inferior parietal lobule	1268	−42	−54	40	4.95
Right pre-supplementary motor area	335	2	18	60	3.21
Left pre-supplementary motor area		−2	18	60	4.44
Right dorsolateral prefrontal cortex	3019	38	20	34	4.01
Left dorsolateral prefrontal cortex	977	−54	20	28	4.08
Region	Condition D				
	Voxels	i	*y*	*z*	*T*-value
Right inferior parietal lobule	2711	46	−66	44	6.81
Left inferior parietal lobule	2898	−64	−48	28	7.66
Right pre-supplementary motor area	2638	2	24	42	6.81
Right anterior mid-cingulate cortex		2	34	32	4.72
Left pre-supplementary motor area		−2	38	50	8.25
Left anterior mid-cingulate cortex		−4	28	36	5.76
Right anterior insular cortex	250	44	14	6	3.82
Left anterior insular cortex	334	−30	18	−6	3.91
Left posterior insular cortex	67	−38	−22	8	4.17
Right dorsolateral prefrontal cortex	3646	40	34	20	6.85
Left dorsolateral prefrontal cortex	2926	−44	38	18	6.99
Left lentiform nucleus	53	−16	10	−6	3.44
Right thalamus	456	4	−12	0	4.15
Left thalamus	79	−4	−14	0	3.50

suggests that S2 is the region specific for mechanically induced cutaneous pain. This notion is supported by the following findings. First, S2 was activated in Condition B and not in Condition D, even though the pressure intensity in Condition D was stronger than that in Condition B. Therefore, the S2 activation does not appear to encode stimulus intensity (Maihofner et al., 2006; Maihofner and Kaltenhauser, 2009). Second, no activation of S2 in Condition A and the significantly stronger activation in Condition B than in Condition A suggest that S2 was activated by nociceptive stimulation, but not by mechanoreceptive stimulation. Last, in previous brain imaging studies, S2 was one of the most consistently activated regions associated with pain limited to the skin and the following: contact heat stimuli (Coghill et al., 1994, 1999; Apkarian et al., 2005), cold stimuli (Davis et al., 2002; Porro et al., 2004) or laser stimuli (Qiu

Table 3
Coordinates (MNI) of the significant differences in Comparison B–A and Comparison D–C.

Region	Comparison B–A				
	Voxels	x	y	z	T-value
Right secondary somatosensory cortex	129	54	−28	26	4.27
Left secondary somatosensory cortex	830	−60	−20	18	8.65
Left posterior insular cortex	59	−36	−16	10	3.54
Right thalamus	273	2	−6	4	5.81
Left thalamus	438	−18	−18	10	3.47
Region	Comparison D–C				
	Voxels	x	y	z	T-value
Right inferior parietal lobule	1651	48	−64	40	6.04
Left inferior parietal lobule	1344	−48	−64	44	5.06
Right pre-supplementary motor area	2071	2	28	42	6.18
Right anterior mid-cingulate cortex		6	34	32	4.36
Left pre-supplementary motor area		−8	26	44	6.45
Left anterior mid-cingulate cortex		−4	28	36	4.38
Left anterior insular cortex	327	−28	20	−4	4.03
Left posterior insular cortex	138	−36	−22	8	4.09
Right dorsolateral prefrontal cortex	1358	40	34	20	4.32
Left dorsolateral prefrontal cortex	1378	−46	32	24	4.84
Right lentiform nucleus	49	14	2	10	4.46
Left lentiform nucleus	263	−12	4	2	4.63
Right thalamus	250	4	14	0	4.79
Left thalamus	411	−6	−26	4	4.79

et al., 2006). On the other hand, a few studies using intramuscular electrical stimulation (IMES) reported that S2 is activated by muscle pain (Svensson et al., 1997; Niddam et al., 2002). The inconsistency may be derived from the inappropriate use of IMES for muscle-specific stimulation (Niddam and Hsieh, 2009). That is, IMES may stimulate both muscle and skin nerve fibers because of its high intensity to induce pain sensation. In addition, muscle and skin twitches accompany IMES. Considering these issues, the pressure stimulation applied in our study shows that S2 is an area specific for cutaneous pain, but not for muscle pain.

4.3. The thalamus

The thalamus was activated in Conditions B and D, in which a nociceptive stimulus was delivered to the skin or the muscle. Since the thalamus is a critical part of the pain matrix, the activation of the thalamus would be associated with pain perception, irrespective of whether the skin or the muscle was stimulated. Another possibility is that the nociceptive stimulus changed the arousal level or non-specific attention (Portas et al., 1998) and the thalamus was thereby activated in Conditions B and D.

4.4. Limitation

The primary somatosensory cortex (S1) was not activated under any conditions in this study using somatosensory mechanical stimuli to the lower leg. Although the reason for the absence of S1 activation is not clear, the most likely explanation seems to be the small somatotopic representation of the lower leg in S1 and the pin head sized stimulation employed in the present study. It is well known that S1 is somatotopically organized and the size of the area representing the lower leg is much smaller than that of the hand (Penfield and Boldrey, 1937). A previous fMRI study, in which thermal stimuli were also applied to the lower leg, reported the absence of activation in S1 by somatosensory stimuli (Oshiro et al., 2007). Therefore, S1 activation by somatosensory stimulation to the calf was not detected, probably because of its small somatotopic mapping.

We did not assess the affective and discriminative components of pain processing, nor did we use graded mechanical stimuli to identify a brain mechanism that encodes stimulus intensity. Instead, we focused on clarifying distinct brain responses by mechanically induced skin versus muscle pain in this study. Therefore, we do not have adequate data to further speculate about the encoding of stimulus intensity or detection and recognition of the noxious nature of nociceptive stimuli.

5. Conclusion

Our results show distinct brain responses to mechanically induced muscle versus skin pain using local anesthesia, which enabled us to induce muscle pain without any accompanying sensation to the skin. We found that the combined activations of aMCC, aIC, pIC, LN, thalamus, DLPFC, IPL and preSMA create a pattern specific for mechanically induced muscle pain, although none of these regions alone seems to be specific for muscle pain. Furthermore, S2 was shown to be an area specific for cutaneous pain but not for muscle pain. These findings reveal a divergence in the pathways for processing tonic muscle and skin pain, and shed light on the neural pathways underlying processing of muscle pain.

Acknowledgements

We thank Tamotsu Nomura for help with imaging procedures, Shigeyuki Kan, Takahiko Koike, Yoshiki Maeda and Yoshitetsu Oshiro for help with image analysis and editing, and Tetsuo Koyama, Masahiko Sumitani and Jeri Helen for manuscript editing. Scans were performed at Ishikawa Hospital.

References

Apkarian, A.V., Bushnell, M.C., Treede, R.D., Zubieta, J.K., 2005. Human brain mechanisms of pain perception and regulation in health and disease. Eur. J. Pain 9, 463–484.

Borsook, D., Moulton, E.A., Tully, S., Schmahmann, J.D., Becerra, L., 2008. Human cerebellar responses to brush and heat stimuli in healthy and neuropathic pain subjects. Cerebellum 7, 252–272.

Coghill, R.C., Talbot, J.D., Evans, A.C., Meyer, E., Gjedde, A., Bushnell, M.C., Duncan, G.H., 1994. Distributed processing of pain and vibration by the human brain. J. Neurosci. 14, 4095–4108.

Coghill, R.C., Sang, C.N., Maisog, J.M., Iadarola, M.J., 1999. Pain intensity processing within the human brain: a bilateral, distributed mechanism. J. Neurophysiol. 82, 1934–1943.

Davis, K.D., Pope, G.E., Crawley, A.P., Mikulis, D.J., 2002. Neural correlates of prickle sensation: a percept-related fMRI study. Nat. Neurosci. 5, 1121–1122.
Graven-Nielsen, T., Mense, S., Arendt-Nielsen, L., 2004. Painful and non-painful pressure sensations from human skeletal muscle. Exp. Brain Res. 159, 273–283.
Helmchen, C., Mohr, C., Erdmann, C., Petersen, D., Nitschke, M.F., 2003. Differential cerebellar activation related to perceived pain intensity during noxious thermal stimulation in humans: a functional magnetic resonance imaging study. Neurosci. Lett. 335, 202–206.
Henderson, L.A., Bandler, R., Gandevia, S.C., Macefield, V.G., 2006. Distinct forebrain activity patterns during deep versus superficial pain. Pain 120, 286–296.
Maihofner, C., Herzner, B., Otto Handwerker, H., 2006. Secondary somatosensory cortex is important for the sensory-discriminative dimension of pain: a functional MRI study. Eur. J. Neurosci. 23, 1377–1383.
Maihofner, C., Kaltenhauser, M., 2009. Quality discrimination for noxious stimuli in secondary somatosensory cortex: a MEG-study. Eur. J. Pain 13, 1048, e1-1048.e7.
Moriguchi, Y., Decety, J., Ohnishi, T., Maeda, M., Mori, T., Nemoto, K., Matsuda, H., Komaki, G., 2007. Empathy and judging other's pain: an fMRI study of alexithymia. Cereb. Cortex 17, 2223–2234.
Niddam, D.M., Yeh, T.C., Wu, Y.T., Lee, P.L., Ho, L.T., Arendt-Nielsen, L., Chen, A.C., Hsieh, J.C., 2002. Event-related functional MRI study on central representation of acute muscle pain induced by electrical stimulation. Neuroimage 17, 1437–1450.
Niddam, D.M., Hsieh, J.C., 2009. Neuroimaging of muscle pain in humans. J. Chin. Med. Assoc. 72, 285–293.
Nie, H., Arendt-Nielsen, L., Andersen, H., Graven-Nielsen, T., 2005. Temporal summation of pain evoked by mechanical stimulation in deep and superficial tissue. J. Pain 6, 348–355.
Oshiro, Y., Quevedo, A.S., McHaffie, J.G., Kraft, R.A., Coghill, R.C., 2007. Brain mechanisms supporting spatial discrimination of pain. J. Neurosci. 27, 3388–3394.
Owen, D.G., Clarke, C.F., Ganapathy, S., Prato, F.S., St Lawrence, K.S., 2010. Using perfusion MRI to measure the dynamic changes in neural activation associated with tonic muscular pain. Pain 148, 375–386.
Penfield, W., Boldrey, E., 1937. Somatic motor and sensory representation in the cerebral cortex of man as studied by electrical stimulation. Brain 60, 389–443.
Peyron, R., Laurent, B., Garcia-Larrea, L., 2000. Functional imaging of brain responses to pain. A review and meta-analysis (2000). Neurophysiol. Clin. 30, 263–288.
Porro, C.A., Lui, F., Facchin, P., Maieron, M., Baraldi, P., 2004. Percept-related activity in the human somatosensory system: functional magnetic resonance imaging studies. Magn. Reson. Imaging 22, 1539–1548.
Portas, C.M., Rees, G., Howseman, A.M., Josephs, O., Turner, R., Frith, C.D., 1998. A specific role for the thalamus in mediating the interaction of attention and arousal in humans. J. Neurosci. 18, 8979–8989.
Qiu, Y., Noguchi, Y., Honda, M., Nakata, H., Tamura, Y., Tanaka, S., Sadato, N., Wang, X., Inui, K., Kakigi, R., 2006. Brain processing of the signals ascending through unmyelinated C fibers in humans: an event-related functional magnetic resonance imaging study. Cereb. Cortex 16, 1289–1295.
Raij, T.T., Numminen, J., Narvanen, S., Hiltunen, J., Hari, R., 2005. Brain correlates of subjective reality of physically and psychologically induced pain. Proc. Natl. Acad. Sci. U.S.A. 102, 2147–2151.
Schreckenberger, M., Siessmeier, T., Viertmann, A., Landvogt, C., Buchholz, H.G., Rolke, R., Treede, R.D., Bartenstein, P., Birklein, F., 2005. The unpleasantness of tonic pain is encoded by the insular cortex. Neurology 64, 1175–1183.
Seifert, F., Jungfer, I., Schmelz, M., Maihofner, C., 2008. Representation of UV-B-induced thermal and mechanical hyperalgesia in the human brain: a functional MRI study. Hum. Brain Mapp. 29, 1327–1342.
Staud, R., Cannon, R.C., Mauderli, A.P., Robinson, M.E., Price, D.D., Vierck Jr., C.J., 2003. Temporal summation of pain from mechanical stimulation of muscle tissue in normal controls and subjects with fibromyalgia syndrome. Pain 102, 87–95.
Suka, M., Yoshida, K., 2005. Musculoskeletal pain in Japan: prevalence and interference with daily activities. Mod. Rheumatol. 15, 41–47.
Sung, E.J., Yoo, S.S., Yoon, H.W., Oh, S.S., Han, Y., Park, H.W., 2007. Brain activation related to affective dimension during thermal stimulation in humans: a functional magnetic resonance imaging study. Int. J. Neurosci. 117, 1011–1027.
Svensson, P., Minoshima, S., Beydoun, A., Morrow, T.J., Casey, K.L., 1997. Cerebral processing of acute skin and muscle pain in humans. J. Neurophysiol. 78, 450–460.
Takahashi, K., Taguchi, T., Itoh, K., Okada, K., Kawakita, K., Mizumura, K., 2005. Influence of surface anesthesia on the pressure pain threshold measured with different-sized probes. Somatosens. Mot. Res. 22, 299–305.
Tracey, I., 2005. Nociceptive processing in the human brain. Curr. Opin. Neurobiol. 15, 478–487.

第3次対がん総合戦略研究事業
「がん性疼痛患者のQOL向上のための橋渡し研究連携拠点の構築」

平成21～23年度

研究成果の刊行物・別冊

Factors Predicting Requirement of High-dose Transdermal Fentanyl in Opioid Switching From Oral Morphine or Oxycodone in Patients With Cancer Pain

Yuko Kanbayashi, PhD, BCOPS,†‡ Toyoshi Hosokawa, MD, PhD,*§ Kousuke Okamoto, PhD,‡ Sawako Fujimoto, CN,* Hideyuki Konishi, MD, PhD,‖ Eigo Otsuji, MD, PhD,¶ Toshikazu Yoshikawa, MD, PhD,‖ Tatsuya Takagi, PhD,‡# Tsuneharu Miki, MD, PhD,** and Masafumi Taniwaki, MD, PhD ††*

Objectives: To identify predictive factors requiring high-dose transdermal fentanyl in opioid switching from oral morphine or oxycodone to transdermal fentanyl in patients with cancer pain.

Methods: The participants were 76 hospitalized terminal cancer patients who underwent opioid switching from oxycodone or morphine sustained-release tablet to transdermal fentanyl at our hospital between January 2009 and June 2010. The conversion dose was calculated as transdermal fentanyl (25 μg/h)/oral morphine (60 mg) or oxycodone (40 mg) = 1. The response evaluated was the dose conversion ratio [transdermal fentanyl/oral morphine or oxycodone (conversion dose to fentanyl)] = Y and was taken to be 0 for $Y \leq 1$, 1 for $1 < Y \leq 2$, 2 for $2 < Y \leq 3$, and 3 for $3 < Y$. Predictors evaluated were factors potentially impacting pain. Ordered logistic regression analysis was carried out to identify the predictive factors requiring high-dose transdermal fentanyl in opioid switching.

Results: Breast cancer [odds ratio (OR) = 8.218; 95% confidence interval (CI), 1.219-55.407; $P = 0.0305$], total protein level (OR = 0.630; 95% CI, 0.408-0.974; $P = 0.0377$), alanine aminotransferase level (OR = 1.017; 95% CI, 1.001-1.033; $P = 0.0390$), advanced age (OR = 3.700; 95% CI, 1.360-10.063; $P = 0.0104$), and male sex (OR = 3.702; 95% CI, 1.355-10.115; $P = 0.0107$) were found to be significant predictive factors requiring high-dose transdermal fentanyl in opioid switching.

Discussion: Our study indicates that breast cancer, total protein, alanine aminotransferase, advanced age, and male sex are significant predictors of a need for higher dose transdermal fentanyl in opioid switching. Our results are considered likely to contribute to the establishment of evidence-based medicine in pain relief and palliative care.

Key Words: transdermal fentanyl, opioid switching, morphine, oxycodone, cancer pain

Received for publication December 12, 2010; revised February 5, 2011; accepted February 19, 2011.

From the Departments of *Pain Treatment and Palliative Care Unit; †Hospital Pharmacy, University Hospital, Kyoto Prefectural University of Medicine; Departments of §Anaesthesiology; ‖Molecular Gastroenterology and Hepatology; ¶Digestive Surgery; **Urology; ††Molecular Hematology and Oncology, Kyoto Prefectural University of Medicine, Graduate School of Medical Science, Kyoto; ‡Pharmainformatics and Pharmacometrics, Graduate School of Pharmaceutical Sciences; and #Genome Information Research Center, Research Institute for Microbial Diseases, Osaka University, Suita, Japan.

The authors declare no conflict of interest.

Reprints: Yuko Kanbayashi, PhD, Department of Hospital Pharmacy, Kyoto Prefectural University of Medicine, Kawaramachi Hirokoji, Kamigyo-ku, Kyoto 602-8566, Japan (e-mail: ykokanba@koto.kpu-m.ac.jp).

(*Clin J Pain* 2011;27:664–667)

Transdermal fentanyl has recently come into common use in patients with cancer pain because of its excellent side effect profile and ease of application.[1–5] Many patients who do not achieve sufficient pain control with transdermal fentanyl, however, fail to attain satisfactory analgesic effect when the dose is increased.[6–8] Such patients may enjoy satisfactory pain control when switched to a morphine or oxycodone product (opioid switching).[8] Patients conversely undergoing opioid switching from an oral morphine or oxycodone product to transdermal fentanyl because of difficulty swallowing may require a higher fentanyl dose than the recommended conversion dose.[9] This has been attributed to terminal cancer patients being unable to absorb substances transdermally and to healthy persons,[10] but the exact causes have not been elucidated. We, therefore, planned this research with the realization that identifying predictive factors requiring high-dose transdermal fentanyl in opioid switching from oral morphine or oxycodone to transdermal fentanyl in patients with cancer pain would help to establish evidence-based medicine for better treatment of cancer pain.

PATIENTS AND METHODS

Study Term and Participants

Patient care records were searched to identify 76 hospitalized terminal cancer patients who underwent opioid switching from oxycodone or morphine-sustained release tablet to transdermal fentanyl at the University Hospital of Kyoto Prefectural University of Medicine between January 2009 and June 2010. This study was carried out with the approval of the ethics review boards of Kyoto Prefectural University of Medicine and Osaka University.

Data Collection

The conversion dose was calculated as transdermal fentanyl (25 μg/h)/oral morphine (60 mg) or oxycodone (40 mg) = 1.[9] The response evaluated was the dose conversion ratio [transdermal fentanyl/oral morphine or oxycodone (conversion dose to fentanyl)] = Y and was taken to be 0 for $Y \leq 1$, 1 for $1 < Y \leq 2$, 2 for $2 < Y \leq 3$, and 3 for $3 < Y$. We extracted the dosage of the following transdermal fentanyl on the opioid switching day 7. Predictors evaluated were factors potentially impacting pain [sex, age, sites of metastasis, body mass index, laboratory test values, and

cancer type]. Laboratory tests that relate to nutritional status, medical condition, hepatic function, and renal function that seemed to influence pain or absorption and pharmacological effects of the transdermal fentanyl were extracted. The retrospective nature of this study made accurate determination of the skin condition of patients difficult, therefore body mass index, which typically decreases as cancer progresses, and nutrition [serum albumin and total protein (TP) levels] were used as alternative indicators of skin condition.

Statistical Analysis

The analytical procedure used was ordered logistic regression, as dose conversion ratio (= response Y) was rated using a graded scale and multiple factors potentially involved in the predictive factors requiring high-dose transdermal fentanyl in opioid switching (= predictors X) had to be evaluated simultaneously. Variables that were highly intercorrelated (correlation coefficient, $r > 0.7$) were excluded because of multicolinearity, which occurs when correlations exist among variables and results in the use of an inappropriate model. One of variables was selected in consideration of correlation strength with response Y or clinical use. A multivariate logistic regression model was constructed using forward stepwise selection among several candidate variables with a variable entry criterion of 0.25 and a variable retention criterion of 0.1. Variables were further screened with the forward selection procedure, after which ordered logistic regression analysis was carried out with the selected variables (JMP 8 software; SAS Institute, Cary, NC). For all statistical analyses, values of $P < 0.05$ (2-tailed) were considered significant.

RESULTS

Table 1 shows characteristics and factors extracted from the 76 patients that may affect doses of transdermal fentanyl in opioid switching. Reasons for switching were difficulty swallowing in 50 patients, nausea/vomiting in 17, drowsiness in 5, decline of renal function in 2, and delirium and intestinal obstruction in 1 patient, respectively. Table 2 shows the conversion ratio in 76 patients, and the 4 categories used. Breast cancer, TP, serum creatinine, bilirubin, alanine aminotransferase (ALT), age, and sex were extracted by forward selection. When multivariate ordered logistic regression analysis was carried out using these variables, breast cancer{[odds ratio (OR) = 8.218; 95% confidence interval (CI), 1.219-55.407; $P = 0.0305$]}TP level (OR = 0.630; 95% CI, 0.408-0.974; $P = 0.0377$). ALT level (OR = 1.017; 95% CI, 1.001-1.033; $P = 0.0390$), advanced age (OR = 3.700; 95% CI, 1.360-10.063; $P = 0.0104$), and male sex (OR = 3.702; 95% CI, 1.355-10.115; $P = 0.0107$) were found to be significant predictors requiring high-dose transdermal fentanyl in opioid switching (Table 3).

TABLE 1. Patient Characteristics and Extracted Factors That May Affect Pain (n=76)

	n (%)	Mean ± SD	Range
Demographic factors			
Sex, (male)	42 (55.3)		
Age, years (≥ 65 y)	38 (50.0)	62.9 ± 14.6	8-85
Physical examination findings			
Bone metastasis	31 (40.8)		
Lymph node metastasis	43 (56.6)		
Peritoneal dissemination	16 (21.1)		
Organ metastasis	41 (53.9)		
BMI		21.0 ± 3.76	12.11-32.76
Laboratory test			
CRP, mg/dL		6.41 ± 6.38	0.03-29.79
ALT, U/L		37.3 ± 62.5	5-492
Albumin, g/dL		2.93 ± 0.62	1.7-4.4
Bilirubin, mg/dL		0.29 ± 0.68	0.14-11.48
Serum creatinine, mg/dL		0.90 ± 0.63	0.16-3.39
Total protein, mg/dL		6.06 ± 1.07	3.9-12.1
Hemoglobin, g/dL		9.13 ± 2.13	4.6-14.8
Daily dosage of opioid			
Oral morphine, mg (n = 5)		30.00 ± 14.14	20-50
Oral oxycodone, mg (n = 71)		26.41 ± 17.99	5-80
Transdermal fentanyl, μg/h (n = 76)		4.64 ± 2.44	1.05-12.6
Type of cancer			
Lung	11 (14.5)		
Gastric	10 (13.2)		
Myeloma	5 (6.6)		
Breast	5 (6.6)		
Colon	4 (5.3)		
Pancreas	4 (5.3)		
Ovarian	4 (5.3)		
Pharyngeal	4 (5.3)		
Esophageal	3 (3.9)		
Melanoma	3 (3.9)		
Bladder	3 (3.9)		
Renal pelvic	3 (3.9)		
Liver	2 (2.6)		
Cholangiocarcinoma	2 (2.6)		
Lymphoma	2 (2.6)		
Renal cellular	2 (2.6)		
Others	9 (11.8)		

ALT indicates alanine aminotransferase; BMI, body mass index; CRP, C-reactive protein.

DISCUSSION

Factors predicting a need for high-dose transdermal fentanyl in opioid switching from oral morphine or oxycodone among patients with cancer pain were breast cancer, TP, high ALT, advanced age, and male sex. Earlier research identified differences in transdermal fentanyl absorption for different diseases.[11,12] Solassol et al[12] stated that there was a significant difference in the percentage of absorbed fentanyl according to the type of cancer and absorption was higher in patients with breast or digestive cancer than in those with lung cancer. In contrast, our study found that breast cancer patients required high-dose transdermal fentanyl when undergoing opioid switching. Patients with advanced breast cancer frequently develop metastasis to bone. Bone metastasis results in intractable pain.[13,14] Breast cancer patients may, therefore, not respond well to fentanyl. This study did not identify metastasis site as a predictive factor. We intend to investigate differences in responses to fentanyl for patients with different diseases further.

TP and ALT were identified as laboratory findings predicting a need for high-dose transdermal fentanyl. Heiskanen et al[10] stated with regard to low TP levels, that

TABLE 2. Categorization of Dose Conversion Ratio

Response (Y)	Dose-conversion Ratio	n (N = 76)
0	$Y \leq 1$	16
1	$1 < Y \leq 2$	37
2	$2 < Y \leq 3$	9
3	$3 < Y$	14

The response evaluated was the dose conversion ratio [transdermal fentanyl/oral morphine or oxycodone (conversion dose to fentanyl)] = Y and was taken to be 0 for $Y \leq 1$, 1 for $1 < Y \leq 2$, 2 for $2 < Y \leq 3$, and 3 for $3 < Y$.

is, poor nutrition, that patients with far advanced cancer often suffered from cachexia, which might have negative effects on the absorption of transdermal fentanyl. The findings in our study agree with earlier research finding that transdermal fentanyl absorption is poor in patients with cachexia. Moreover, fentanyl is metabolized by the drug-metabolizing enzyme CYP3A4 present in the liver, and therefore must be used with care when given in combination with CYP3A4 inhibitors, as such combinations have been shown to result in elevated blood concentrations.[15–17] Other studies, however, have found that the efficacy of fentanyl is unaffected by liver disease[18] and that fentanyl drug sensitivity differs among individuals.[19] The effects of high ALT levels and other liver function markers on response to fentanyl must be further clarified.

Advanced age was identified as a predictive factor. Earlier research has also found that transdermal fentanyl absorption worsens with advancing age.[12,20,21] Decreasing moisture content of the skin with aging is thought to decrease transdermal fentanyl absorption. Solassol et al[12] stated that bioavailability of fentanyl differed significantly according to patient age. Patients older than 75 years absorbed 50% of the fentanyl during the selected 72-hour period, whereas patients younger than 65 years absorbed 66%. Our results support those findings.

Male sex was identified as a predictive factor. As for cancer pain, an earlier study clarified that pain was significantly exacerbated when the patient was male.[14] Gupta et al,[22] however, found no sex-based differences in transdermal fentanyl absorption. Yet, other studies have stated that women absorb transdermal fentanyl less effectively and require higher doses because of higher levels of subcutaneous fat.[23] The impact of sex requires further characterization.

TABLE 3. Results of Ordered Logistic Regression Analysis for Variables Extracted by Forward Selection (Accuracy=45/76)

			CI of Odds Ratio	
Variable	P	Odds Ratio	Lower 95%	Upper 95%
Breast cancer	0.0305*	8.218	1.219	55.407
TP	0.0377*	0.630	0.408	0.974
sCr	0.1123	0.546	0.258	1.1525
T-bil	0.18	0.822	0.618	1.095
ALT	0.0390*	1.017	1.001	1.033
Age	0.0104*	3.700	1.360	10.063
Sex	0.0107*	3.702	1.355	10.115

*$P < 0.05$.

ALT indicates alanine aminotransferase; CI, confidence interval; sCr, serum creatinine; T-bil, total bilirubin; TP, total protein.

In conclusion, we used a statistical approach to identify factors predicting a need for higher dose transdermal fentanyl in opioid switching from oral morphine or oxycodone in patients with cancer pain. Our study indicates that breast cancer, TP, ALT, advanced age, and male sex are significant predictors of a need for higher dose transdermal fentanyl in opioid switching. Our study has limitations in terms of the retrospective nature of the investigation and the relatively small number of patients analyzed. 95% CI shows a very wide range especially in breast cancer, so our results have a limitation in precision. But the statistical identification of predictors for higher dose transdermal fentanyl in opioid switching is considered likely to contribute to the establishment of evidence-based medicine in pain relief and palliative care.

REFERENCES

1. Radbruch L, Sabatowski R, Loick G, et al. Constipation and the use of laxatives: a comparison between transdermal fentanyl and oral morphine. *Palliat Med*. 2000;14:111–119.
2. Ripamonti C, Fagnoni E, Campa T, et al. Is the use of transdermal fentanyl inappropriate according to the WHO guidelines and the EAPC recommendations? A study of cancer patients in Italy. *Support Care Cancer*. 2006;14:400–407.
3. Morita T, Takigawa C, Onishi H, et al. Opioid rotation from morphine to fentanyl in delirious cancer patients: an open-label trial. *J Pain Symptom Manage*. 2005;30:96–103.
4. Allan L, Hays H, Jensen NH, et al. Randomised crossover trial of transdermal fentanyl and sustained release oral morphine for treating chronic non-cancer pain. *BMJ*. 2001;322:1154–1158.
5. Menten J, Desmedt M, Lossignol D, et al. Longitudinal follow-up of TTS fentanyl use in patients with cancer-related pain: results of a compassionate use study with special focus on elderly patients. *Curr Med Res Opin*. 2002;18:488–498.
6. Benítez-Rosario MA, Feria M, Salinas-Martín A, et al. Opioid switching from transdermal fentanyl to oral methadone in patients with cancer pain. *Cancer*. 2004;101:2866–2873.
7. Mercadante S, Ferrera P, Villari P, et al. Rapid switching between transdermal fentanyl and methadone in cancer patients. *J Clin Oncol*. 2005;23:5229–5234.
8. Clemens KE, Klaschik E. Clinical experience with transdermal and orally administered opioids in palliative care patients—a retrospective study. *Jpn J Clin Oncol*. 2007;37:302–309.
9. Donner B, Zenz M, Tryba M, et al. Direct conversion from oral morphine to transdermal fentanyl: a multicenter study in patients with cancer pain. *Pain*. 1996;64:527–534.
10. Heiskanen T, Mätzke S, Haakana S, et al. Transdermal fentanyl in cachectic cancer patients. *Pain*. 2009;144:218–222.
11. Van Nimmen NF, Poels KL, Menten JJ, et al. Fentanyl transdermal absorption linked to pharmacokinetic characteristics in patients undergoing palliative care. *J Clin Pharmacol*. 2010;50:667–678.
12. Solassol I, Caumette L, Bressolle F, et al. Inter- and intra-individual variability in transdermal fentanyl absorption in cancer pain patients. *Oncol Rep*. 2005;14:1029–1036.
13. Cicek M, Oursler MJ. Breast cancer bone metastasis and current small therapeutics. *Cancer Metastasis Rev*. 2006;25:635–644.
14. Kanbayashi Y, Okamoto K, Ogaru T, et al. Statistical validation of the relationships of cancer pain relief with various factors using ordered logistic regression analysis. *Clin J Pain*. 2009;25:65–72.
15. Armstrong SC, Wynn GH, Sandson NB. Pharmacokinetic drug interactions of synthetic opiate analgesics. *Psychosomatics*. 2009;50:169–176.
16. Saari TI, Laine K, Neuvonen M, et al. Effect of voriconazole and fluconazole on the pharmacokinetics of intravenous fentanyl. *Eur J Clin Pharmacol*. 2008;64:25–30.

17. Kharasch ED, Whittington D, Hoffer C. Influence of hepatic and intestinal cytochrome P4503A activity on the acute disposition and effects of oral transmucosal fentanyl citrate. *Anesthesiology*. 2004;101:729–737.
18. Tegeder I, Lötsch J, Geisslinger G. Pharmacokinetics of opioids in liver disease. *Clin Pharmacokinet*. 1999;37:17–40.
19. Zhang W, Chang YZ, Kan QC, et al. CYP3A4*1G genetic polymorphism influences CYP3A activity and response to fentanyl in Chinese gynecologic patients. *Eur J Clin Pharmacol*. 2010;66:61–66.
20. Otis J, Rothman M. A phase III study to assess the clinical utility of low-dose fentanyl transdermal system in patients with chronic nonmalignant pain. *Curr Med Res Opin*. 2006;22:1493–1501.
21. Thompson JP, Bower S, Liddle AM, et al. Perioperative pharmacokinetics of transdermal fentanyl in elderly and young adult patients. *Br J Anaesth*. 1998;81:152–154.
22. Gupta SK, Hwang S, Southam M, et al. Effects of application site and subject demographics on the pharmacokinetics of fentanyl HCl patient-controlled transdermal system (PCTS). *Clin Pharmacokinet*. 2005;44:25–32.
23. Björkman S, Stanski DR, Verotta D, et al. Comparative tissue concentration profiles of fentanyl and alfentanil in humans predicted from tissue/blood partition data obtained in rats. *Anesthesiology*. 1990;72:865–873.

Journal of Neurochemistry

JOURNAL OF NEUROCHEMISTRY | 2011 | 118 | 256–265 doi: 10.1111/j.1471-4159.2011.07297.x

ORIGINAL ARTICLE

Pre-emptive morphine treatment abolishes nerve injury-induced lysophospholipid synthesis in mass spectrometrical analysis

Jun Nagai and Hiroshi Ueda

Division of Molecular Pharmacology and Neuroscience, Nagasaki University Graduate School of Biomedical Sciences, Nagasaki, Japan

Abstract

We have previously demonstrated that lysophosphatidic acid (LPA) production in the spinal cord following partial sciatic nerve injury (SCNI) and its signaling initiate neuropathic pain. In order to examine whether LPA production depends on the intense nociceptive signal, we have attempted to see suppression by pre-emptive treatment with centrally administered morphine, which mainly inhibits nociceptive signal at the level of spinal cord. In the present study, we developed a quantitative mass spectrometry assay to simultaneously analyze several species of lysophosphatidyl choline (LPC). The levels of 16:0-, 18:0- and 18:1-LPC in the spinal cord and dorsal root were maximally increased at 75 min after SCNI and then declined, as LPC is converted to LPA by autotaxin (ATX). In $atx^{+/-}$-mice, on the other hand, these levels were similar to wild-type mice at 75 min, but maximal at 120 min, suggesting that this difference is partly due to the low conversion of LPC to LPA in $atx^{+/-}$-mice. When morphine was centrally administered before SCNI, the injury-induced increase of LPC was completely abolished. These results suggest that LPC (or LPA) is produced by injury-induced nociceptive signal, which is effectively and pre-emptively suppressed by central morphine, possibly through known descending anti-nociceptive pathways.

Keywords: autotaxin, lysophosphatidyl choline, mass spectrometry, morphine, neuropathic pain, pre-emptive analgesia.

J. Neurochem. (2011) **118**, 256–265.

Lysophosphatidic acid (LPA) plays various physiological or pathophysiological roles as one of lipid mediators (Noguchi *et al.* 2009; Choi *et al.* 2010; Chun *et al.* 2010; Lin *et al.* 2010; Ueda 2011). This lipid mediator is synthesized in biological fluids including blood from lysophosphatidylcholine (LPC) by autotaxin (ATX), possessing lysophospholipase D activity (Tokumura 2002; Aoki *et al.* 2008). Although significant amounts of ATX are also present in the CSF, the levels of LPC and LPA are very low, suggesting that extracellular LPC production would be a rate-limiting step for LPA production (Nakamura *et al.* 2009). Recently, we have demonstrated that LPA is produced in the spinal cord (SC) (Ma *et al.* 2010b) and its LPA_1 receptor signaling initiates neuropathic pain and underlying mechanisms including demyelination in the dorsal root (DR), $Ca_v\alpha2\delta1$ up-regulation in the dorsal root ganglion (DRG) and protein kinase Cγ in the spinal cord, all which are supposed to contribute to neuropathic allodynia and hyperalgesia (Inoue *et al.* 2004; Ueda 2006, 2008, 2011). As the antagonistic blockade of LPA_1 receptor for 2–3 h after the injury abolished successive long-lasting abnormal pain (Ma *et al.* 2009a), LPA production is supposed to initiate neuropathic pain. Thus, we have currently focused on the LPA production in *in vitro* and *in vivo* studies (Inoue *et al.* 2008b; Ma *et al.*

Received January 23, 2011; revised manuscript received April 29, 2011; accepted May 2, 2011.

Address correspondence and reprint requests to Hiroshi Ueda, Division of Molecular Pharmacology and Neuroscience, Nagasaki University Graduate School of Biomedical Sciences, 1-14 Bunkyo-machi, Nagasaki 852-8521, Japan. E-mail: ueda@nagasaki-u.ac.jp

Abbreviations used: ATX, autotaxin; $atx^{+/-}$, mice heterozygous for *atx* gene; DR, dorsal root; DRG, dorsal root ganglion; LPA, lysophosphatidic acid; LPC, lysophosphatidyl choline; NALDI-TOF-MS, nanostructure-assisted laser desorption/ionization time-of-flight mass spectrometry; PLA_2, phospholipase A2; SC, spinal cord; SCNI, partial sciatic nerve injury; WT, wild-type.

2010a; b). In these studies, LPA levels have been measured as cell-rounding activities in B103 cells expressing LPA_1 receptor. LPA levels are increased only in the ipsilateral side of the dorsal half of SC and DR after partial sciatic nerve injury (SCNI), and the peak effects were observed at 3 h (Ma *et al.* 2010b). As ATX is largely lost in the *in vitro* studies using spinal cord slices, we have added recombinant ATX in the incubation medium and measured LPA, which had been converted from LPC. The elevation of LPA levels in spinal cord slices was reproduced only by the combination of different types of pain transmission by substance P and NMDA as an intense nociceptive model (Inoue *et al.* 2008b). Thus, it is hypothesized that the production of LPA, an initiator of neuropathic pain may occur by intense nociceptive signal to SC.

It is accepted that morphine exerts potent analgesia by driving descending anti-nociceptive system from midbrain periaqueductal gray matter or rostroventromedial medulla to spinal dorsal horn (Sato and Takagi 1971; Basbaum and Fields 1979; Fields *et al.* 2006). Based on the view that neuropathic pain is formed by a kind of memory-processes (Zhuo 2007), we have successfully demonstrated that the central pre-treatment with morphine to prevent the intense nociceptive input abolished long-lasting neuropathic pain (Rashid and Ueda 2005). This finding may provide the important evidence to support the existence of pre-emptive analgesia (Richmond *et al.* 1993). In the present study, we report the simultaneous quantitation method for multiple species of LPC by use of nanostructure-assisted laser desorption/ionization time-of-flight mass spectrometry (NALDI-TOF-MS) system and demonstrate the evidence for the prevention of LPC (as the LPA precursor) production by pre-emptive morphine treatment.

Materials and methods

Animals

Male mutant mice for the *atx* gene ($atx^{+/-}$) mice (Tanaka *et al.* 2006) and their sibling wild-type (WT) mice from the same genetic background (C57BL/6J), weighing 20–24 g, were used. They were housed at room temperature (21 ± 2°C) with free access to a standard laboratory diet and tap water. The procedures were approved by the Nagasaki University Animal Care Committee and complied with the recommendations of the International Association for the Study of Pain (Zimmermann 1983).

Partial ligation of sciatic nerve

Partial ligation of the sciatic nerve was performed under pentobarbital (50 mg/kg) anesthesia, according to the methods of Malmberg and Basbaum (1998). Briefly, the common sciatic nerve of the right hind limb was exposed at high thigh level through a small incision and the dorsal half of the nerve thickness was tightly ligated with a silk suture. A sham-operation was performed similarly except without touching the sciatic nerve.

Extraction of LPC from tissues

The unilateral dorsal half including dorsal horn (laminae I–V) of the lumber (L4–L6) spinal cord (SC) and L4–L6 DRs on the ipsilateral or contralateral side were then removed to enable the extraction of LPC as reported previously (Ma *et al.* 2009a; b). The averaged wet weights of the isolated unilateral SC and DRs in each mouse were 8 and 4 mg tissue weight, respectively. LPC were extracted from tissues according to modified methods (Sutphen *et al.* 2004). After their isolation, the tissue sample was placed in 1.5-mL tubes and homogenized by sonication in 250 μL of phosphate-buffered saline for approximately 30 s. The homogenates were then mixed with 1 mL of methanol/chloroform (2 : 1) and 30 μL of 10 N HCl were added in a glass tube (13 × 100 mm IWAKI). The samples were vortexed for 1 min and incubated on ice for 10 min. Chloroform (0.5 mL) and water (0.5 mL) were added for the formation of the two-phase system of the Bligh and Dyer method in acidic conditions (Bligh and Dyer 1959). The mixture was centrifuged at 2000 *g* for 10 min, and the chloroform phase was collected, and the remaining water/methanol phase was mixed with 0.5 mL of chloroform for another extraction. Subsequently, the chloroform phases were combined, dried with N_2 gas. The final sample was dissolved in as less as 50 μl of methanol and stored at −80 °C until use for analysis.

Nanostructure-assisted laser desorption/ionization time-of-flight mass spectrometry analyses

One microliter from 50 μL of finally obtained methanol solution was diluted with methanol (DR: 200–400 μL, SC: 400–600 μL) to adjust the concentration to the standard curve levels. One microliter of the sample including internal standard deuterium-labeled stearoyl (18:0)-LPC (D35-LPC) in a dose of 0.1 pmol (Doosan Serdary Research Laboratories, London, Canada) was spotted on the NALDI plate (Bruker Daltonics, Inc., Billerica, MA, USA). After drying, the sample was applied to an Ultraflexi™ TOF/TOF systems (Bruker Daltonics, Inc.). Mass spectrometry was performed in the reflector mode, using an accelerating voltage of 25 kV. The laser energy was used at energy of 10–20% (1.0–2.0 μJ) and a repetition rate of 10 Hz. The mass spectra were calibrated externally using PEG 600 (Nacalai Tesque, Kyoto, Japan) as a standard peptide calibration. Each spectrum was produced by accumulating data from 300–500 consecutive laser shots. Standards of LPC were purchased from Sigma Chemical (St Louis, MO, USA) for 16:0-, 18:0- and 18:1-LPC, from Doosan Serdary Research Laboratories (London, Canada) for 18:2-, 18:3- and 20:4-LPC.

Identification of lysophosphatidyl choline species

In MS/MS analysis, mass spectra were acquired in LIFT mode using an UltraflexIII™ TOF/TOF systems (Bruker Daltonics, Inc.). The laser was used from 40% (4.0 μJ) to 60% (6.0 μJ). The mass spectra were obtained from ipsilateral spinal dorsal horn after nerve injury. Structure determination of lipid molecules was performed using lipid databases, such as LIPID MAPS (http://www.lipidmaps.org/) and the Lipid Search (http://lipidsearch.jp/), according to previous reports (Hsu and Turk 2003; Pulfer and Murphy 2003; Koizumi *et al.* 2010).

Statistical analysis

The differences between multiple groups were analyzed by one-way ANOVA with Tukey's multiple comparison *post hoc* analysis (Figs 5

and 7). The criterion of significance was set at $^*p < 0.05$. All results are expressed as the mean ± SEM.

Results

Standard curve of lysophosphatidyl choline species by NALDI-TOF-MS

The NALDI plate is layered with nano-structured coating, which serves as an active matrix-free surface for desorption/ionization of spotted samples. The NALDI technique is optimal for the analysis of small molecules, such as LPC, because of low background (Wyatt *et al.* 2010). Typical charts of mass spectra with authentic standard reagents, 16:0-, 18:0-, 18:1-LPC, and internal standard D35-LPC at the level of 0.1 pmol/well were shown (Fig. 1a and c). However, the dose-related linearity of the ratios of ion-peak heights with each standard (16:0-, 18:0-, 18:1-, 18.2-, 18:3- and 20:4-LPC) at 0.01–1.0 pmol/well to the one with fixed D35-LPC (0.1 pmol/well) were shown (Fig. 1d and i). In this analysis, the signal derived from authentic species of LPC molecules was calculated by subtracting the basal background. The equation for linearity of 16:0-, 18:0-, 18:1-, 18:2-, 18:3- and 20:4-LPC levels were $y = 1441.5x$ ($R^2 = 0.982$), $y = 439.0x$ ($R^2 = 0.986$), $y = 922.3x$ ($R^2 = 0.976$), $y = 194.1x$ ($R^2 = 0.949$), $y = 1913.9x$ ($R^2 = 0.986$) and $y = 922.6x$ ($R^2 = 0.989$), respectively. The detection efficiency of 18:2-LPC was much lower than the others, although it remains what causes the difference.

Recovery yields of authentic LPC species

To examine the recovery yield of LPC through extraction and partial purification processes, 2 nmol of authentic 16:0-, 18:0- and 18:1-LPC were added to the tissue homogenates. Purified materials (in 50 μL methanol solution) were diluted by 400-fold volume of methanol, and 1 μL was plotted to the NALDI-TOF-MS plate (Fig. 2a and b). However, 0.1 pmol each of standard LPC mixture was analyzed as a control (Fig. 2c). When the LPC level was evaluated after adjusting to a standard curve, the recovery yield of LPC species was 70.6 ± 5.3% ($n = 4$) for 16:0-LPC, 85.1 ± 2.1% ($n = 4$) for 18:0-LPC and 89.6 ± 6.2% ($n = 4$) for 18:1-LPC, respectively.

Nerve injury-induced increase in the levels of LPC species in the spinal cord

The unilateral dorsal horn of the lumber spinal cord was isolated at 75 min after the partial injury of right sciatic

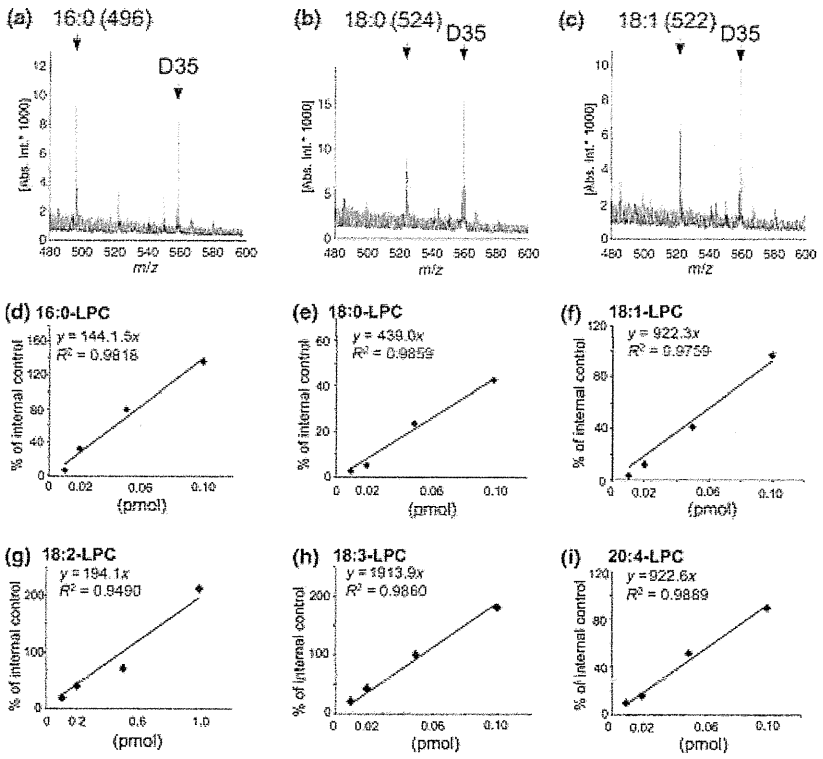

Fig. 1 Standard curve of LPC species by NALDI-TOF-MS. (a–c) Representative charts of mass spectra with authentic standard reagents, 16:0-, 18:0-, 18:1-LPC, and internal standard D35-LPC at the level of 0.1 pmol/well. (d–i) Dose-related signal level of lysophosphatidyl choline (LPC) homologues as compared with corresponding internal standards. Different amounts (0.01–1 pmol) of 16:0-LPC (d), 18:0-LPC (e), 18:1-LPC (f), 18:2-LPC (g), 18:3-LPC (h) and 20:4-LPC (i) were mixed with a fixed amount of D35 LPC (0.1 pmol) in 1 μL of methanol and subjected to NALDI-TOF-MS.

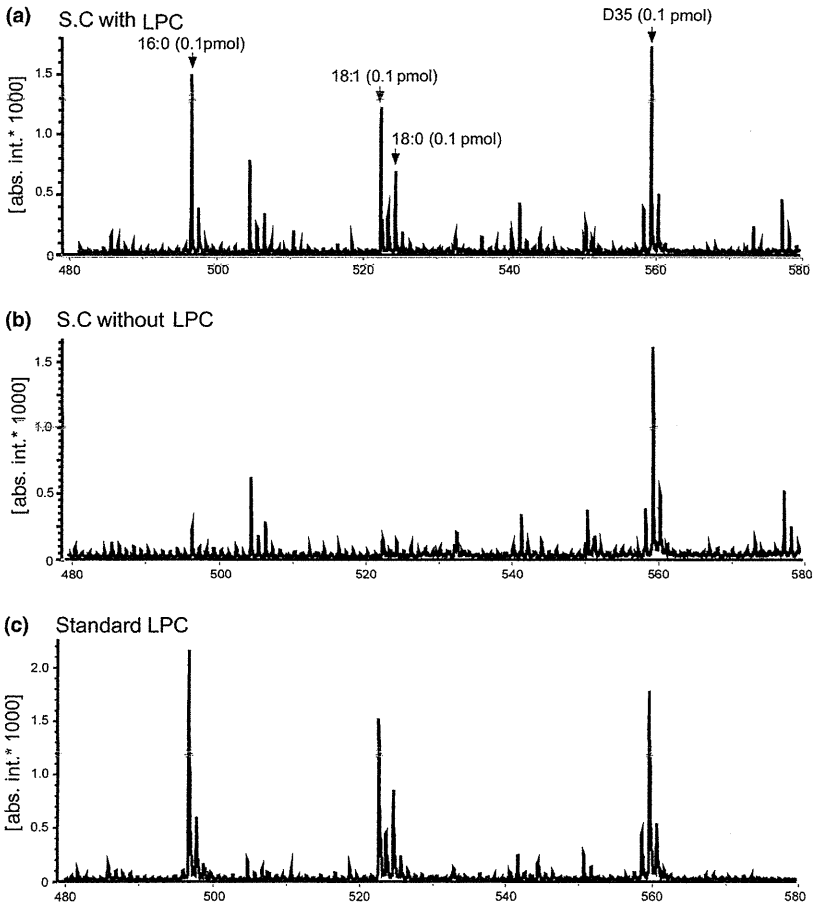

Fig. 2 Recovery yields of authentic LPC species. Representative charts of mass spectra of partially purified samples from the spinal dorsal horn with or without authentic standard: Results represent the mass spectra of partially purified materials from the dorsal half of spinal cord. NALDI-TOF-MS analysis was performed using an Ultraflexl™ TOF/TOF systems in positive ion mode. Numbers above ion peaks indicate their *m/z* values. (a) Authentic LPC mixture (16:0-, 18:0-, and 18:1-LPC) in a dose of 2 nmol each was added to the homogenates of spinal cord. To adjust the concentration to a standard curve levels, 1 μL from 50 μL of finally obtained methanol solution was diluted with 400 μL of methanol. One microliter of the sample applied on NALDI-TOF-MS analysis. (b) Authentic LPC was not added to the homogenates. (c) Standard LPC mixture (0.1 pmol each) was spotted to the NALDI-plate with finally purified materials. The internal standard D35-LPC in a dose of 0.1 pmol was spotted to the plate in all samples.

nerve, followed by homogenization in phosphate-buffered saline and methanol/chloroform extraction. The sample was used for NALDI-TOF-MS analysis. The representative mass spectra of the samples from contralateral (control side) or ipsilateral (injured side) spinal cord are shown (Fig. 3). Marked increases in the ion-signal were observed at m/z 496, 522, 524 and 578 (Fig. 3). Although the signal at *m/z* 504 was decreased (Fig. 3b), this change was not reproduced after repeated trials.

Structure determination of LPC species by MS/MS analysis

MS/MS analyses were performed to determine the structure of molecular ions. When the signal at *m/z* 496 was applied with stronger laser energy at 4.0–6.0 μJ, fragment signals at *m/z* 104, derived from choline, m/z 184, derived from phosphocholine and m/z 313, derived from 16:0 monoacyl glycerol in addition to the original one at *m/z* 496 (Fig. 4a). By use of the database search of the LIPID MAPS and the Lipid Search as previously reported (Hsu and Turk 2003; Pulfer and Murphy 2003; Koizumi *et al.* 2010), the signal at *m/z* 496 was deduced as 16:0-LPC. Similar analysis applied to *m/z* 524 also revealed that there were three fragment signals at *m/z* 104, 184 and 341, and it was deduced as 18:0-LPC (Fig. 4b). Although stronger laser energy treatment of the signal at *m/z* 522 produced fragment signal at 104 and 184, but not the residual signal at *m/z* 339 derived from monoacyl glycerol, it could be also deduced as 18:1 LPC (Fig. 4c).

Time-dependent elevation of nerve injury-induced production of LPC

When the ipsilateral side of spinal cord was isolated at various time points up to 180 min after the nerve injury, there was a significant increase in the level of 16:0-LPC only at 75 min (Fig. 5a). However, there was no significant change on the contralateral side of spinal cord. As autotaxin (ATX), which has lysophospholipase D activity and converts LPC to LPA, plays a key role in nerve injury-induced LPA production (Aoki *et al.* 2008; Ma *et al.* 2010b), we used $atx^{+/-}$-mice to study the effect of ATX on the LPC production. The injury-induced increase in 16:0-LPC was further enhanced in the preparation from the ipsilateral spinal cord from $atx^{+/-}$-mice, but not from the contralateral preparation. The peak effect was observed at 120 min after

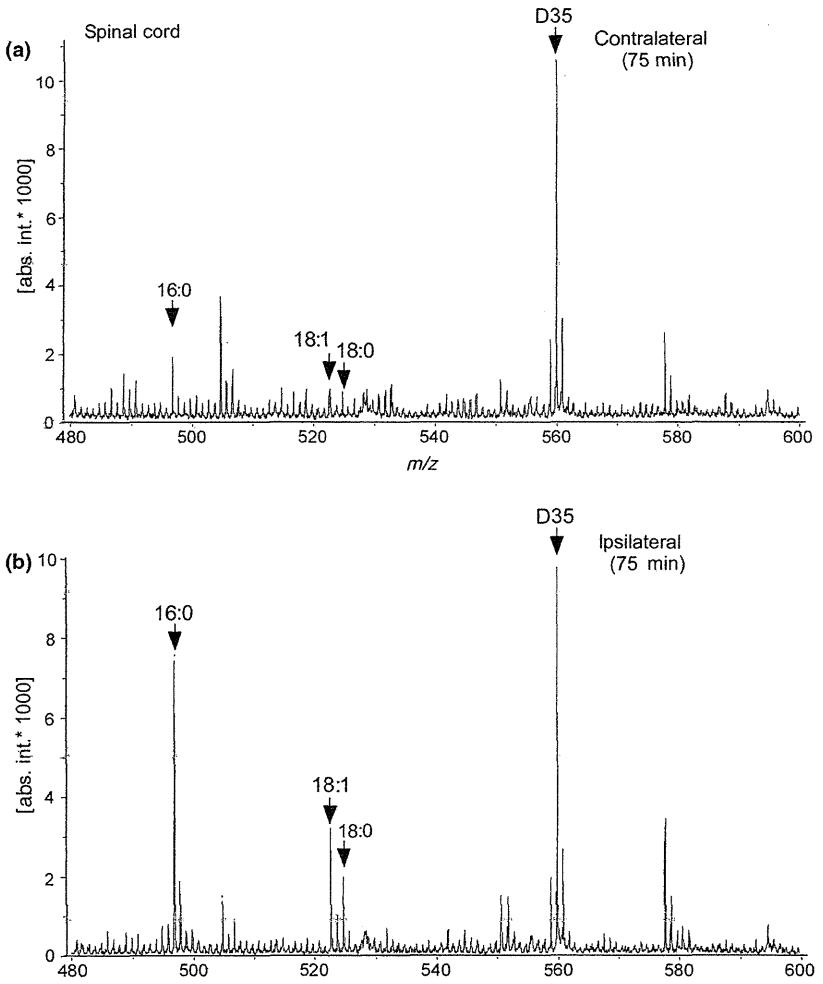

Fig. 3 Biosynthesis of LPC following nerve injury. Representative charts of mass spectra of spinal dorsal horn samples from mice treated with or without SCNI. Results represent the mass spectra of partially purified materials from the contralateral (a) and ipsilateral dorsal half (b) of spinal cord at 75 min after nerve injury.

the injury. The maximum level of 16:0-LPC from $atx^{+/-}$-mice was 240 pmol/mg tissue, which was higher than that from WT-mice (202 pmol/mg tissue). However, the levels at 75 min from $atx^{+/-}$- and WT-mice were equivalent. Quite similar changes were also observed in the cases with 18:0-LPC and 18:1-LPC (Fig. 5b and c).

In the dorsal root, however, injury-induced increase in the preparation from WT mice was also maximal at 75 min in all three species of LPC (Fig. 5d and f). These changes were calculated as 50–100 pmol/mg tissue, which are slightly lower than the case with spinal cord. The peak effect in LPC production at the dorsal root of $atx^{+/-}$-mice was also observed at 120 min, but the increase was less than the case with spinal cord.

When the levels of three species of LPC (16:0-, 18:0- and 18:1-LPC) were combined, the conclusion became clearer. The peak-time increase in LPC following injury in both spinal cord and dorsal root of WT mice was 75 min after the nerve injury. As shown in Fig. 5g and h, the injury increased the LPC level from 308 (at 0 min) to 552 pmol/mg tissue (at 75 min) in the spinal cord (8 mg tissue) of WT mice, while from 288 (at 0 min) to 450 pmol/mg tissue (at 75 min) in the dorsal root (4 mg tissue). Thus, the increase in LPC levels in the spinal cord of WT mice was calculated to be approximately three times higher than that in the dorsal root, and the levels in both spinal cord and dorsal root of $atx^{+/-}$-mice at 120 and 180 min appear to be higher than those in WT mice, although no significant change was observed at 75 min.

Morphine pre-treatment blocks nerve injury-induced LPC production

When morphine at a dose of 3 nmol/5 μL was intracerebroventricularly administered 30 min prior to the nerve injury, nerve injury-induced increase in 16:0-, 18:0- and 18:1-LPC production at 75 min in the spinal cord was all abolished, while there were no significant changes in other ion-peaks (Fig. 6). Quantitative analyses revealed that the morphine pre-treatment completely abolished the injury-induced production of these three LPC species in the dorsal root as well as spinal cord (Fig. 7).

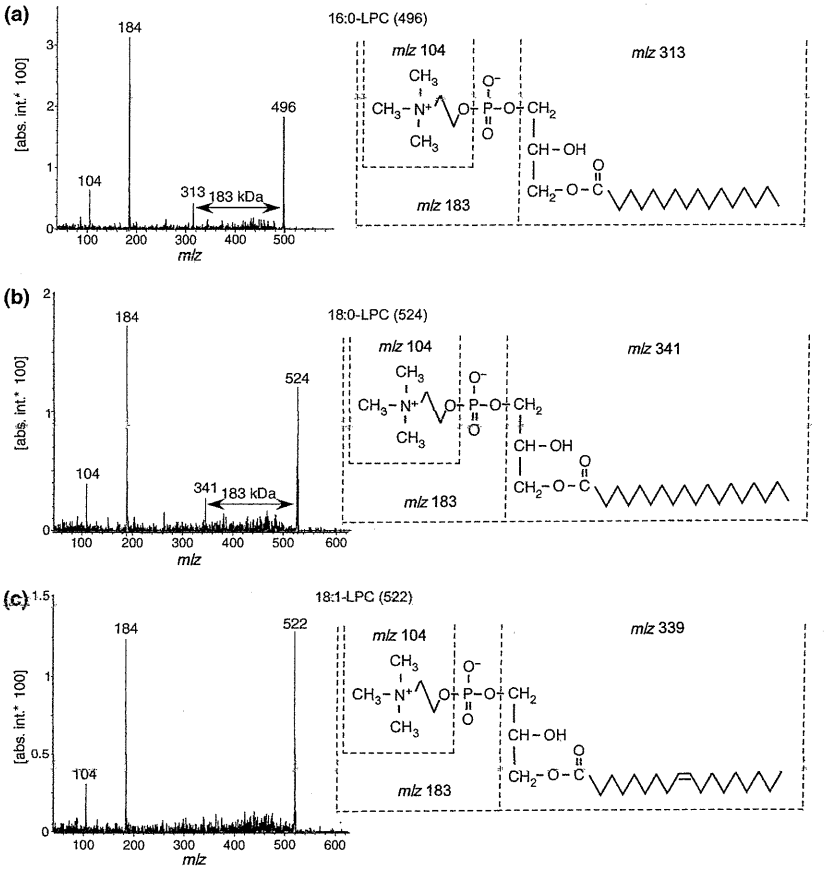

Fig. 4 Structure determination of LPC species by MS/MS analysis MS/MS analyses of ion peaks at *m/z* 496 (a), *m/z* 524 (b), *m/z* 522 (c), obtained from the spinal cord samples with SCNI. Results represent spectra of product ions (left panels) and determined structures deduced by database search (right panel).

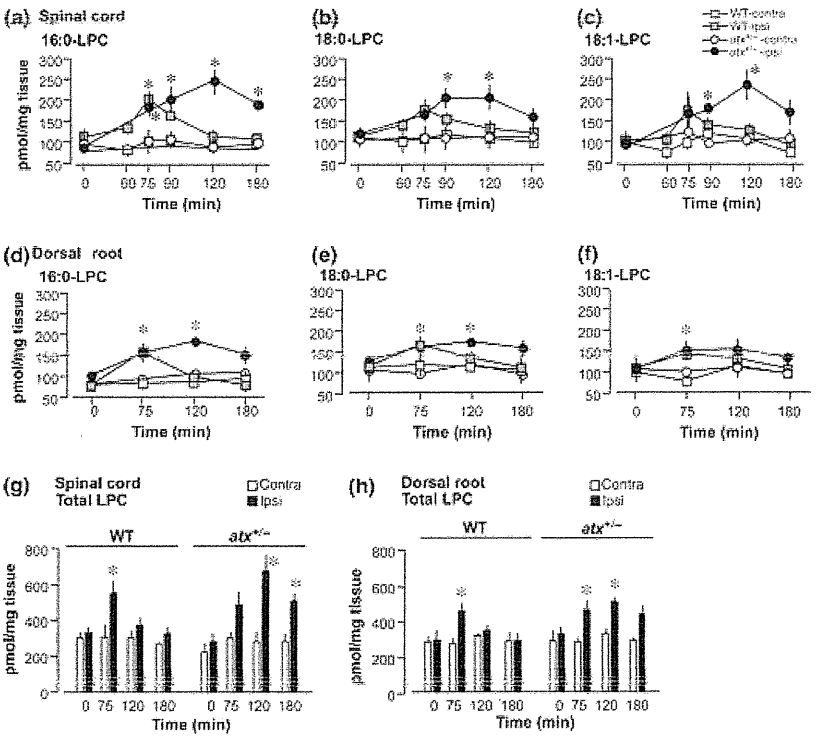

Fig. 5 Time course of LPC levels in spinal cord and dorsal root following nerve injury of WT or *atx*$^{+/-}$ -mice. (a–f) The contents of each species of LPC (16:0-, 18:0-, 18:1-LPC) as pmol/mg tissue weight of spinal cord (a–c) or dorsal root (d–f) preparations at various time-points after the injury of WT and *atx*$^{+/-}$ mice were quantified. (g, h) The combined contents of three LPC species from spinal cord (g) or dorsal root (h) were quantified. Data are expressed as the mean ± SEM from experiments using 3–6 mice. *$p < 0.05$, versus contralateral preparations.